Chapter 5

LOW-TEMPERATURE DYNAMIC SPIN FREEZING IN $Er_2Ti_{2-x}Mn_xO_7$

5.1 Introduction

In the preceding chapter, we studied the role of Mn in modifying optical and electronic properties of Ising pyrochlore, i.e., $Dy_2Ti_{2-x}Mn_xO_7$ (x = 0.00, 0.05, 0.10, 0.15, & 0.20). We investigated this through theoretical (density functional theory calculations) and experimental (ultraviolet-visible absorption and photoluminescence emission spectroscopy and Raman spectroscopy) approaches. In further chapters, we have studied the role of Mn substitution on the magnetic, structural, optical, and electronic properties of another class of system, an XY-type pyrochlore, i.e., $Er_2Ti_2O_7$. $Er_2Ti_2O_7$ has been proposed as ⟨111⟩ XY antiferromagnet pyrochlore. The spins of Er^{3+} lie perpendicular to the local ⟨111⟩ axis. The order of energy for the magnetic interactions present in such a system are low, as are the magnetic ordering temperatures when present. Thus, the systems are expected to be very sensitive to small perturbations of all kinds, including those relevant to the symmetry of the magnetic system.

This chapter presents the structural and low-temperature static and dynamic magnetic properties of $Er_2Ti_2O_7$ as well as the impact of partial inclusion of Mn at the Ti site, i.e., represented as $Er_2Ti_{2-x}Mn_xO_7$ (x = 0, 0.1, 0.2).

5.2 Structural Analysis

The structure of $Er_2Ti_2O_7$ is described by the cubic space group $Fd\bar{3}m$, comprising a network of corner-sharing tetrahedra with Er^{3+} ions in their corners. $Er_2Ti_2O1_6O2$ is the preferable formula with an anti-prismatic arrangement of the six oxygen atoms around the central Er ion. The Er, Ti, O1, and O2 occupy the Wyckoff sites 16d (1/2,1/2,1/2), 16c (0, 0, 0), 48f (x, 1/8, 1/8), and 8b (3/8, 3/8, 3/8) respectively [143]. The local symmetry of the rare earth site is defined by two equidistant oxygen atoms oriented along the ⟨1,1,1⟩ axis, while the remaining six oxygen atoms lie in a plane perpendicular to this axis, forming a distorted hexagon. These local anions arrangements determine the magnetic symmetry of the rare earth site (involving an axial term and a planar term, which can both play a role) [1], [3].

When this pyrochlore lattice is stuffed with Mn ions at the Ti site, it gets distorted due to the change in oxygen sublattices surrounding the Er (16d) and Ti (16c) sites. The oxygen environment around the Er^{3+} ion and Ti ion is given in **Figure 5.1**. The only refinable parameter, x, will characterize this degree of distortion in the structure. Its ramification can be strongly seen in the bond angle (O1-Ti-O1) of the TiO_6 octahedron [137], [144]. In the context of pyrochlore structure, a perfect cube of oxygen environment would have a value of x = 0.375. This is also responsible for influencing the dynamic of spin freezing at a lower temperature. So, the consequences of this distortion are reflected in the lattice parameter, volume and bond lengths (Er-O1, Er-O2, Er-Er, Ti-O2), bond angles (O1-Er-O1, O1-Er-O2, Ti-O1-Ti, O1-Ti-O1) all of which decreases with the increasing value of substituent concentration (Mn) as given in **Table 5.1.** The substituted Mn^{4+} cations of smaller ionic radii (~0.67Å, 6-coordinates) occupied the Ti^{4+} cation site of larger ionic radii (~0.74Å, 6-

coordinates) almost in the same amount [145]. Correspondingly, the MnO_6 octahedra are smaller than the existing TiO_6 octahedra. Therefore, we realized a slight decrease in the lattice parameter based on ionic radii difference consistent with the reported literature.

Rietveld refinement of the HRXRD pattern of $Er_2Ti_2O_7$ and its Mn-doped form $Er_2Ti_{2-x}Mn_xO_7$ was carried out using the FULLPROF Suite. The room temperature high-resolution x-ray diffraction (HRXRD) pattern and the Rietveld refinement of $Er_2Ti_{2-x}Mn_xO_7$ is shown in **Figure 5.2**. The observed, calculated, and difference patterns, as well as the allowed reflection peaks, are shown in **Figure 5.2**, and all the reflection peaks are indexed according to the calculated profile for $Fd\bar{3}m$ space group. No additional phase could be detected. The crystallographic information, such as lattice parameters, bond length and bond angles obtained from Rietveld refinement of the HRXRD pattern, are listed in **Table 5.1.**

Table 5.1 Lattice parameters Bond length and bond angles of $Er_2Ti_{2-x}Mn_xO_7$ (x = 0, 0.10, 0.20) series obtained from Rietveld refinement of HRXRD data

Compound $Er_2Ti_{2-x}Mn_xO_7$	Experimental lattice parameter(Å)	Refinable parameter (x,0,0)	Bond Length (Å)				Bond Angle (°)		
			Er-O1	Er-O2	Ti-O2	Er-Er	O1-Er-O2	O1-Er-O1	O1-Ti-O1
x = 0	10.0811(5)	0.3276(3)	2.489(3)	2.1826(0)	1.9462(13)	3.5642(0)	79.55(5)	63.22(3)	95.80(11)
x = 0.10	10.0779(6)	0.3262(4)	2.498(3)	2.1819(0)	1.9400(16)	3.5630(3)	79.78(7)	63.08(4)	95.30(15)
x = 0.20	10.0729(6)	0.3264(4)	2.496(3)	2.1808(0)	1.9398(16)	3.5613(3)	79.74(7)	63.10(4)	84.62(15)

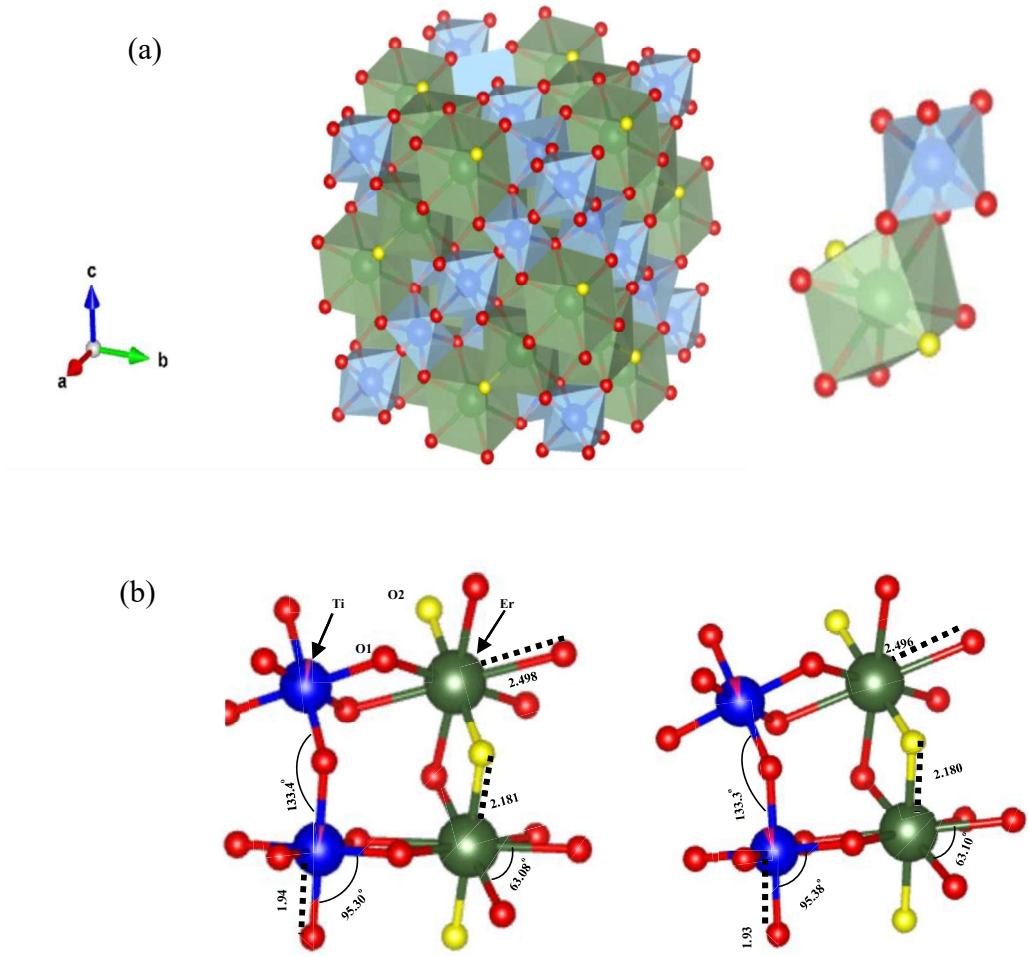

Figure 5.1 (a) Oxygen environment around rare-earth ion and Ti ion formed by O1 and O2 in $Er_2Ti_{2-x}Mn_xO_7$ (b) Schematic illustration of bond length and bond angles.

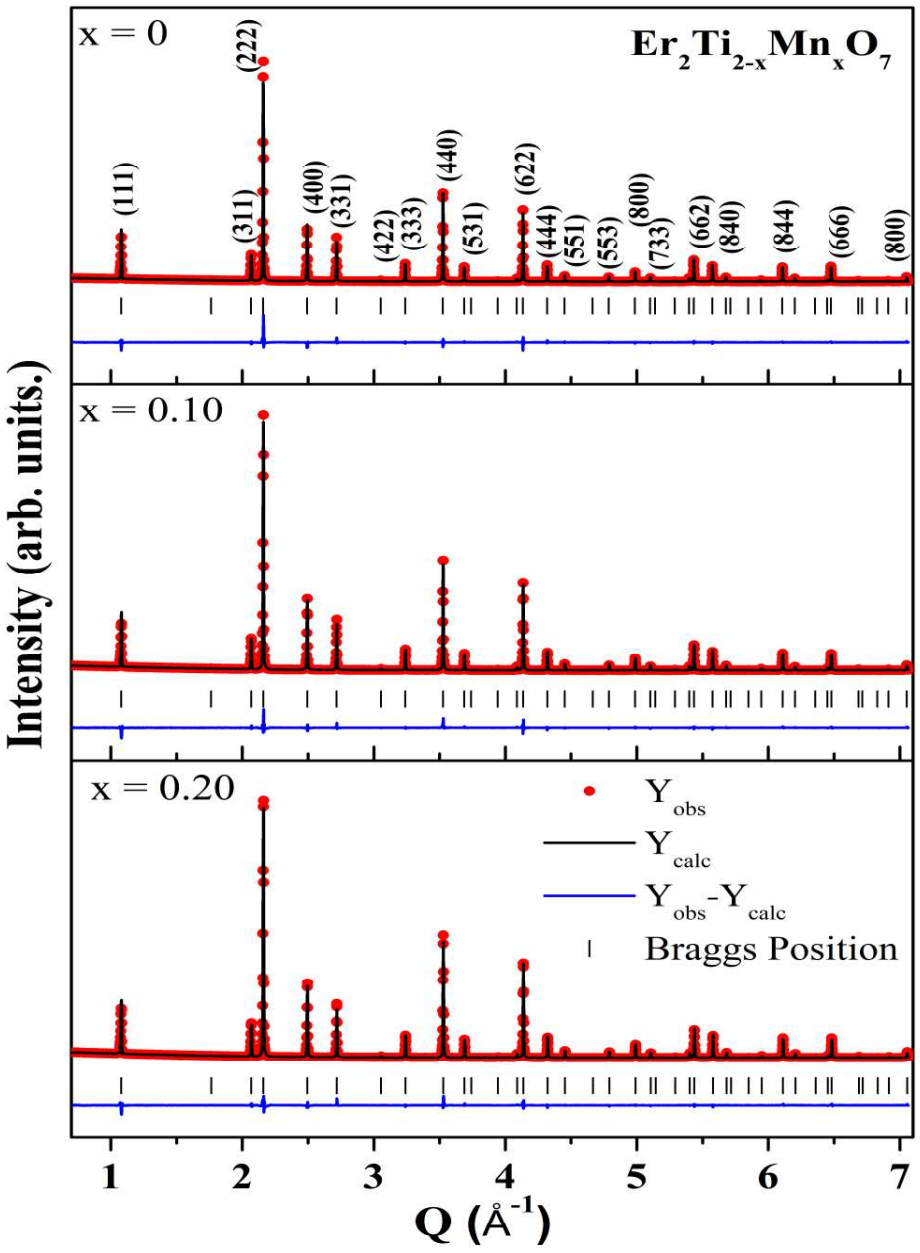

Figure 5.2 Room temperature HXRD Pattern for $Er_2Ti_{2-x}Mn_xO_7$ (x = 0, 0.10, 0.20) Observed (solid red circles), calculated (solid black line) and difference (below blue line) HXRD pattern.

5.2.1 Role of Mn substitution on the structure

The effect of increasing Mn concentration can be seen in **Figure 5.3,** which shows the shift of (222) and (311) peaks towards higher Q value with an increase in x from 0 to 0.20 in $Er_2Ti_{2-x}Mn_xO_7$. It clearly indicates shrinkage in the lattice parameter. The sequential reduction in lattice parameter (obtained from Rietveld refinement) is shown pictorially in **Figure 5.4.**

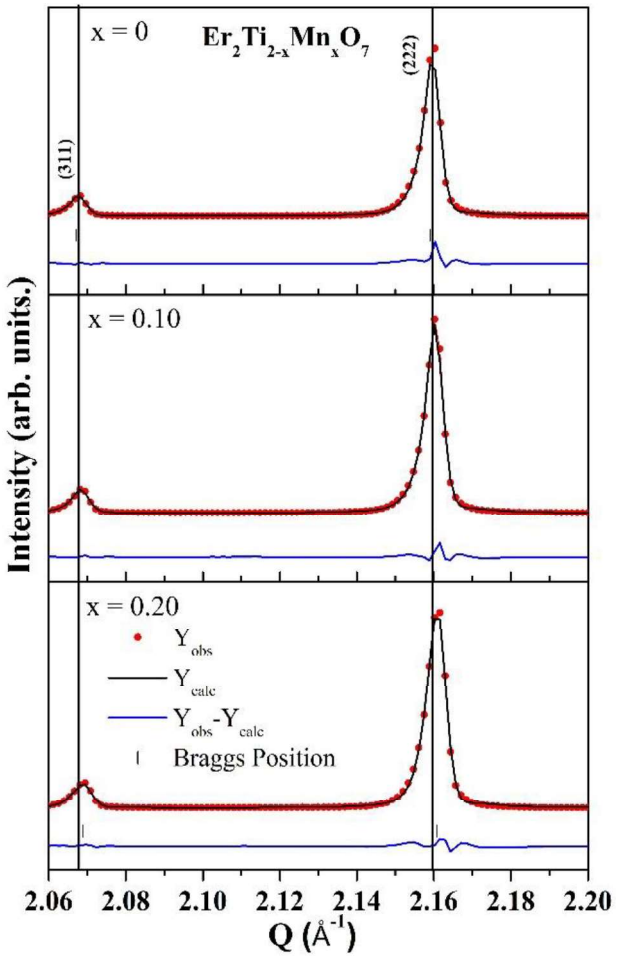

Figure 5.3 Room temperature high resolution x-ray diffraction data (HRXRD) indicating the shift of (222), (311) peaks towards higher Q value and with increase in chemical pressure for $Er_2Ti_{2-x}Mn_xO_7$(x = 0, 0.10, 0.20)

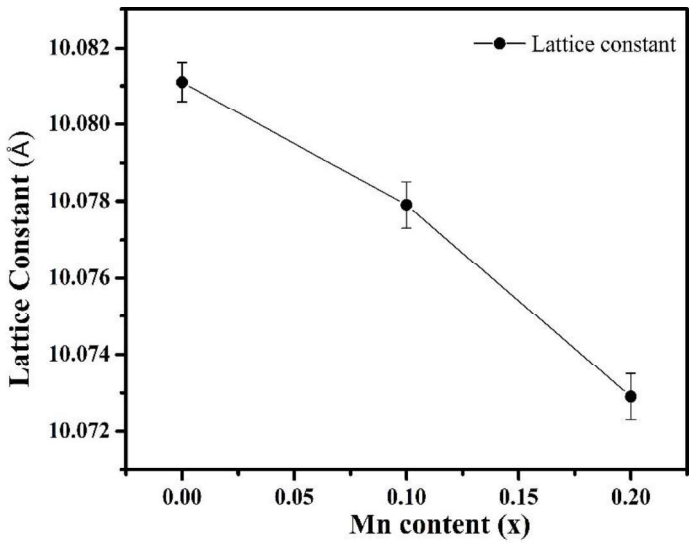

Figure 5.4 Variation of lattice parameter with x for $Er_2Ti_{2-x}Mn_xO_7$ (x = 0, 0.10, 0.20)

5.3 Magnetic Properties

5.3.1 Temperature-dependent magnetization

Temperature dependence dc susceptibility measurement, M(T) for $Er_2Ti_{2-x}Mn_xO_7$ has been performed at an applied field of 100 Oe and 1000 Oe in zero-field-cooled (ZFC) mode and field-cooled (FC) mode. The magnetization was measured between 2-200 K. M(T) curve shows that the magnetization increases with a decrease in temperature down to 2 K, and no transition is observed down up to 2 K for all the composition, as shown in **Figure 5.5**.

The sharp increase in magnetization at lower temperatures can be attributed to magnetic interactions such as dipolar and exchange interactions dominant at lower temperatures. The same magnetic response is observed in ZFC and FC mode for 100 Oe and 1000 Oe; the ZFC and FC curves overlap. Further, with an increase in Mn concentration, the low-temperature

increase in magnetization becomes sharper. It is possibly because of Mn changing the interactions present at low temperatures.

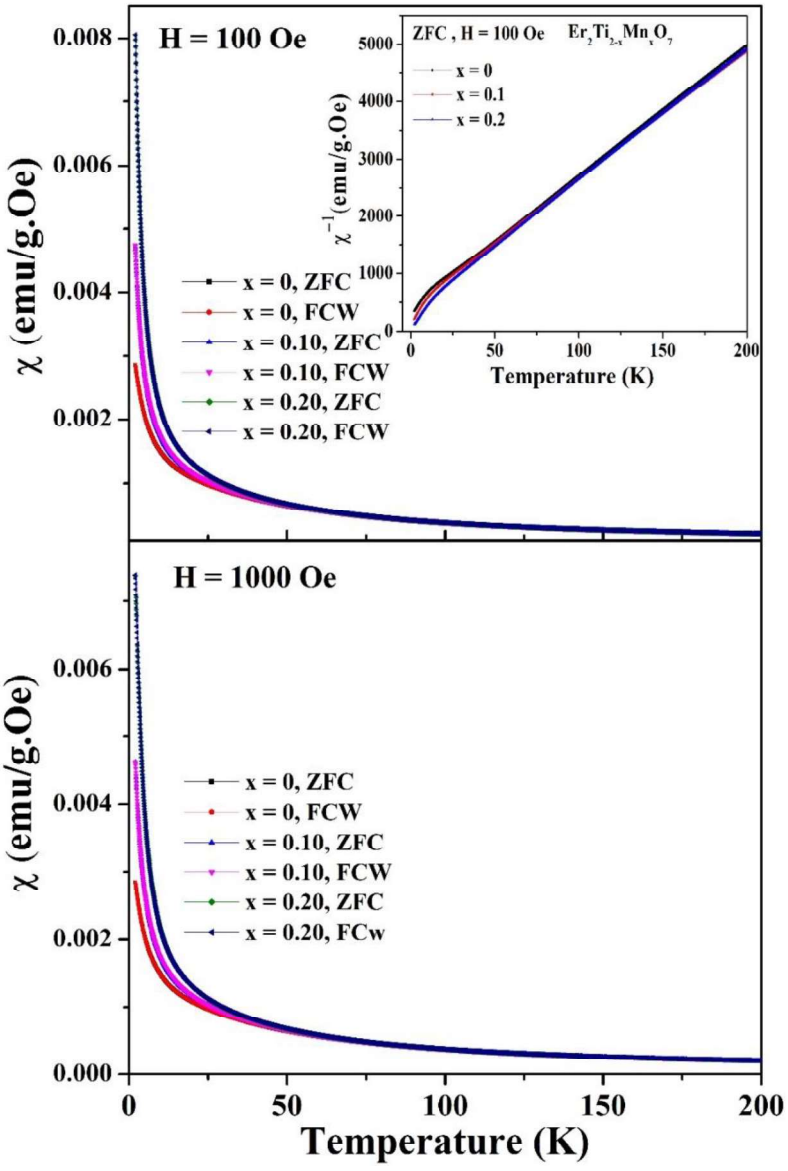

Figure 5.5 Temperature dependence of dc magnetic susceptibility curve of $Er_2Ti_{2-x}Mn_xO_7$ (x = 0.0, 0.10, 0.20) in zero -field-cooling and field-cooling mode. Inset shows the inverse of magnetic susceptibly curve obtained from dc susceptibility for ZFC data to derive Curie-Weiss temperature by fitting Curie-Weiss law for $Er_2Ti_{2-x}Mn_xO_7$.

Classically, the dc Magnetic susceptibility χ is expected to follow Curie-Weiss law far from the ordering temperature in the paramagnetic regime.

$$\chi(T) = \frac{N_A \mu_{eff}^2}{(3\, k_B(\mathrm{T} - \theta_{cw}))} \quad (5.1)$$

Where θcw is the Curie-Weiss temperature, μ_{eff} is the effective magnetic moment, k_B is the Boltzmann constant, and N_A is the Avogadro number. High-temperature Curie-Weiss linear fitting of χ^{-1}-T plot shown in the inset of **Figure 5.5,** obtained from temperature variation of magnetization data. The Curie-Weiss temperature obtained from this fitting is given in **Table 5.2.** The negative θ_{cw} signifies that the dominant exchange interaction is antiferromagnetic [43]. The values of θ_{cw}, obtained by fitting χ^{-1}(T) in the temperature range 25 K – 65 K, are listed in the table. The obtained values of θ_{cw} are consistent with previous reports [43], [146], [147]. It can be seen that θ_{cw} becomes less negative as we increase the Mn concentration. This tendency of increase in the value of θ_{cw} with an increase in Mn substitution is indicative of the decrease in AFM interaction, though overall interaction remains AFM.

Table 5.2 The obtained values of θcw from Curie-Weiss linear fitting of χ^{-1} vs. temperature.

Compound	**θ_{cw} (K); H=100 Oe**
$Er_2Ti_2O_7$	-17.08
$Er_2Ti_{0.1}Mn_{1.9}O_7$	-16.87
$Er_2Ti_{0.2}Mn_{1.8}O_7$	-13.54

5.3.2 Field dependent magnetization

Figure 5.6 shows the field dependence of magnetization, M-H, for $Er_2Ti_{2-x}Mn_xO_7$ (x = 0.0, 0.10, 0.20) at 2 K. The experimental procedure was to first cool the sample to 2 K in zero magnetic fields, and the field was swept up to 50 kOe, down to − 50 kOe, and back up to 50 kOe to complete the hysteresis loop. M-H curve shows the antiferromagnetic-like behavior. The magnetization measured in the paramagnetic state of $Er_2Ti_2O_7$ reveals a smooth increase of magnetic moment, which is not saturated in the external field up to 5 T [146]–[148]. The magnetization increases with increasing Mn concentration. This trend is consistent with the fact that we have substituted Mn, a magnetic ion, at a non-magnetic Ti site.

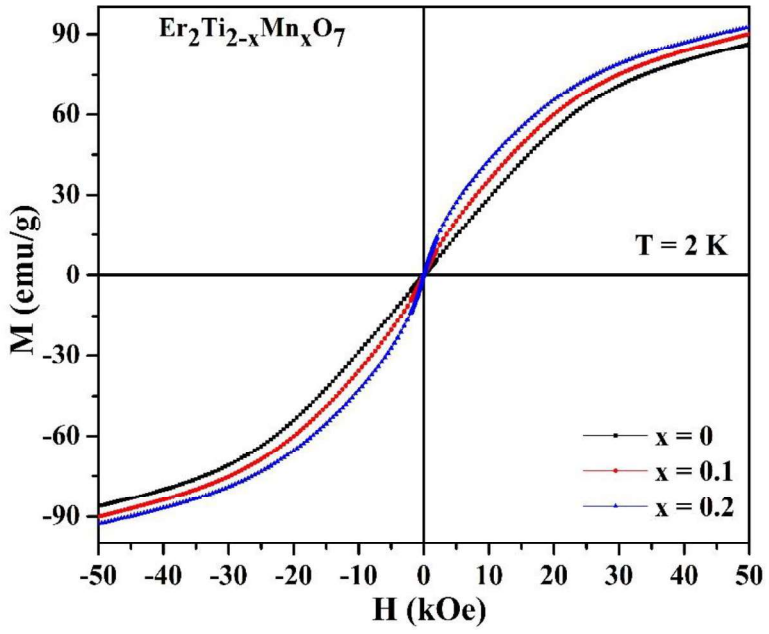

Figure 5.6 Magnetization as a function of field (M-H) curve for $Er_2Ti_{2-x}Mn_xO_7$ at various temperatures for H (magnetic field) ranging from -50 kOe to 50 kOe.

5.3.3 Temperature-dependent ac-susceptibility

To study the relaxation process, we performed ac-susceptibility measurement in temperature ranging from 2 K to 40 K at various applied dc bias magnetic fields at a frequency of 300 Hz. **Figure 5.7** shows the real parts of the field-dependent ac susceptibility, $\chi'(T)$, for $Er_2Ti_{2-x}Mn_xO_7$.

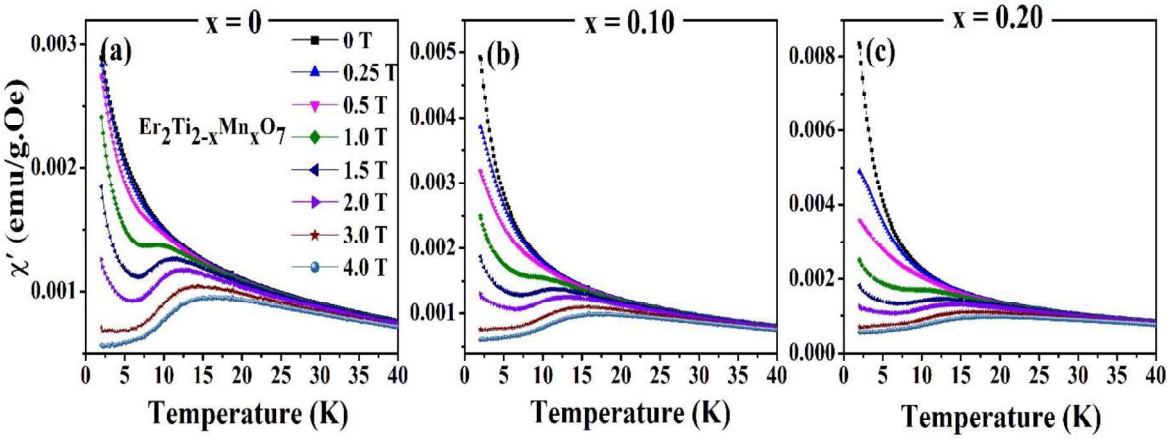

Figure 5.7 Temperature dependence of the real part of ac susceptibility measured at the 300 Hz frequency for $Er_2Ti_{2-x}Mn_xO_7$ (x = 0.0, 0.10, 0.20) at different DC bias fields (a) x = 0 (b) x = 0.10 (c) x = 0.20.

Although there is no prominent transition is seen in dc susceptibility data down to 2 K, we observed an emergence of a peak in ac-susceptibility measurement around 15 K with increasing the dc bias field, H > 1 T in the case of $Er_2Ti_2O_7$ as shown in **Figure 5.7**. At H = 0, $\chi'(T)$ closely follows the canonical paramagnetic behavior, i.e., monotonically rising with an increasing slope as the temperature decreases. By contrast, data taken in a field are more complex. We observe the emergence of a peak at T = 15 K in $\chi'(T)$ for fields H > 0.5 T, which becomes more pronounced and shifts to higher temperatures with increasing field. Similar

results have been observed for x= 0.1 and x= 0.2 compounds, but this peak suppresses and shifts towards the higher temperature side with an increase in Mn concentration. The high field peak in $\chi'(T)$ is a consequence of single moment saturation since the susceptibility associated with thermal spin fluctuations must approach zero both at high temperatures and as $T \rightarrow 0$ in the presence of a strong enough field [149].

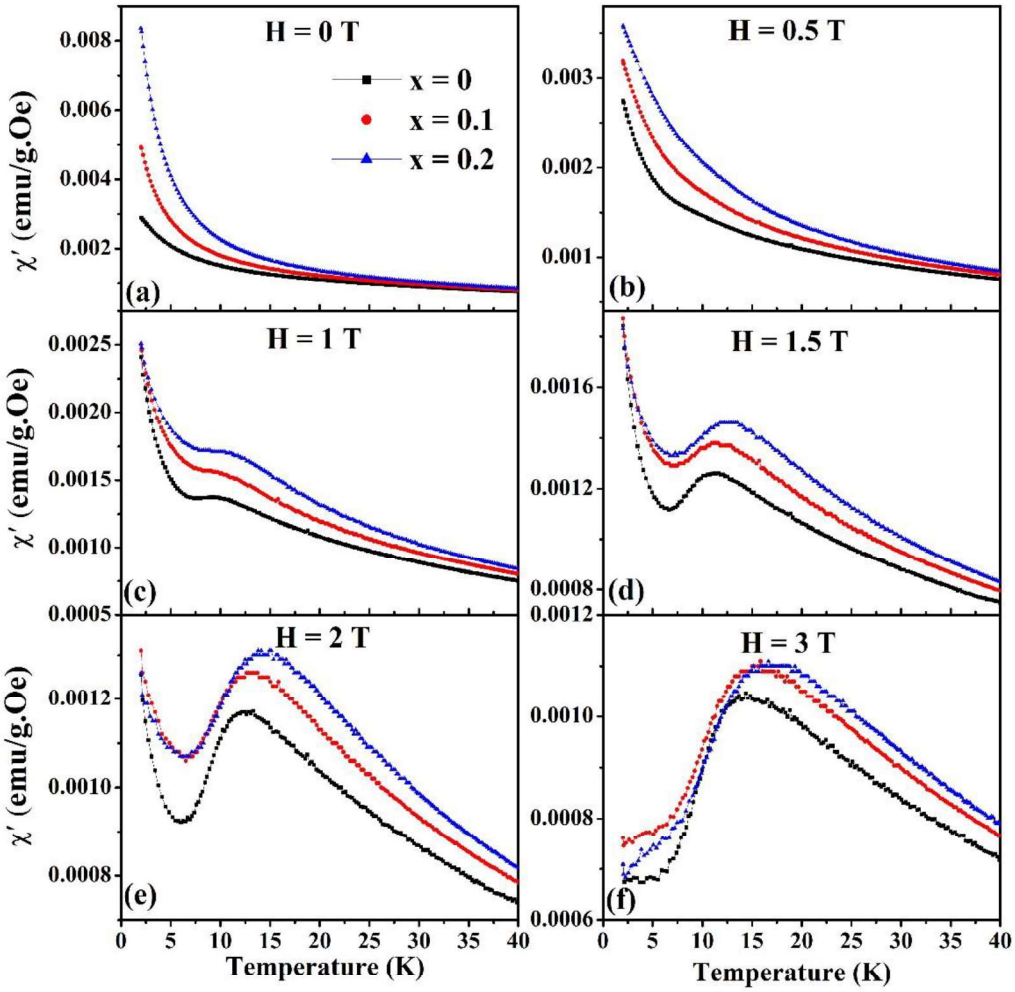

Figure 5.8 Temperature dependence of the real part of ac susceptibility measured at the 300 Hz frequency for $Er_2Ti_{2-x}Mn_xO_7$ (x = 0.0, 0.10, 0.20) at different DC bias fields (a) 0 T (b) 0.5 T (c) 1 T (d) 1.5 T (e) 2 T (f) 3 T

Further, to analyze the role of Mn inclusion, ac susceptibility for $Er_2Ti_{2-x}Mn_xO_7$ (x = 0.0, 0.10, 0.20) is plotted in the single figure at the various applied fields, as shown in **Figure 5.8**. The gradual increment of applied dc-magnetic field, its effect on spin freezing, and the effect of Mn doping is studied. **Figure 5.8 (a)** shows the ac susceptibility data in the absence of dc magnetic field, which did not show any spin freezing, but with the increase in the applied dc bias magnetic field to 0.5 T, there is an emergence of spin freezing around 15 K as shown in **Figure 5.8(b).** With further increasing field to 1.5 T as depicted in **Figure 5.8 (d)** this freezing becomes more pronounced in case of $Er_2Ti_2O_7$ and with increase in Mn concentration from x= 0.1 to x= 0.2 this peak suppresses and shifts towards the higher temperature side**.** Since Mn is magnetic, it can affect the magnetic interactions between the magnetic moments and the crystal field environment around the magnetic ion.

5.4 Conclusions

In summary, we have investigated the structural and the low-temperature magnetic properties of the $Er_2Ti_{2-x}Mn_xO_7$ pyrochlore system. The ac susceptibility study reveals evidence of spin-freezing in $Er_2Ti_2O_7$. This high field spin freezing peak in $\chi'(T)$ is a consequence of single moment saturation. This spin freezing becomes more pronounced with the increase in the applied dc-magnetic field. Further, we have studied the effect of Mn doping on the Ti site in $Er_2Ti_2O_7$. With the increase in Mn concentration from x = 0.1 to x = 0.2, this peak suppresses and shifts towards the higher temperature side.